

Imaging of nanostructures with sub-100 nm spatial resolution using a desktop EUV microscope

Przemysław W. Wachulak · Andrzej Bartnik ·
Henryk Fiedorowicz · Dalibor Pánek ·
Petr Brůža

Received: 29 November 2011 / Revised: 9 April 2012 / Published online: 16 September 2012
© The Author(s) 2012. This article is published with open access at Springerlink.com

Abstract Laser-produced plasma sources of short-wavelength radiation offer an interesting alternative to synchrotron and free-electron laser installations. Recently, we reported on a newly developed desktop EUV microscope based on plasma generated from a gas-puff target and diffractive optics. The half-pitch resolution of the microscope approached 50 nm. Compared to analogous microscopes based on synchrotron sources, our system is compact and cost-effective. In this paper, we present the results of imaging experiments on a thin polycrystalline object that was carried out in order to further examine the applicability of the microscope. We have demonstrated here that EUV microscopy can provide structural information that cannot be accessed by conventional optical microscopy or SEM.

1 Introduction

Recent rapid developments of nanoscience and nanotechnology require nanometer scale resolution imaging tools and methods. One of the methods, extensively studied for the last few decades, is an extreme ultraviolet (EUV) and soft X-ray (SXR) microscopy, based on Fresnel zone plates [1]. Photon-based EUV/SXR microscopy is capable of reaching resolutions down to 12 nm using synchrotron radiation [2]. However, the complicacy and extreme financial demands associated with measurements on synchrotrons leads to the existing demand for more affordable sources of short-wavelength radiation. The introduction of compact sources of bright EUV and SXR radiation paved the way for the development of tabletop microscopes that can render images of nanoscale objects with exposures as short as a few seconds and spatial resolution approaching that of synchrotron-based microscopes [3–5].

Many imaging experiments were carried out to date using smaller-scale EUV and SXR sources, such as high-order harmonics [6], SXR lasers [7], and incoherent laser-plasma based sources [8]. A 13.2-nm wavelength radiation from Ni-like Cd EUV laser allowed for a 55 nm in reflection mode [9] and sub-38 nm resolution nano-imaging in transmission mode with standard test objects such as various pitch gratings [3]. A capillary discharge EUV laser was employed for imaging of an entanglement of 50 nm diameter carbon nanotubes with spatial resolution approaching that of wavelength of illumination $\lambda = 46.9$ nm and temporal resolution of ~ 1 ns [10]. Quasi-monochromatic emission from an incoherent SXR source based on liquid nitrogen, $\lambda = 2.88$ nm, in the so-called “water window” range, allowed to demonstrate SXR microscopy with sub-50 nm spatial resolution [11]. Finally, using a xenon-based gas discharge EUV source, a Schwarzschild objective and a

P. W. Wachulak (✉) · A. Bartnik · H. Fiedorowicz
Institute of Optoelectronics,
Military University of Technology,
ul. gen. S. Kaliskiego 2,
00-908 Warsaw, Poland
e-mail: wachulak@gmail.com

A. Bartnik
e-mail: abartnik@wat.edu.pl

H. Fiedorowicz
e-mail: hfiedorowicz@wat.edu.pl

D. Pánek · P. Brůža
Faculty of Biomedical Engineering,
Czech Technical University in Prague,
Nám. Sítná, 3105 Kladno, Czech Republic
e-mail: panekdal@fbmi.cvut.cz

P. Brůža
e-mail: bruzapet@fbmi.cvut.cz

Fresnel zone-plate for the second magnification step, EUV imaging was demonstrated reaching the spatial resolution of ~ 100 nm [12].

In this paper, we report on an application of a desktop microscopy using a laser-plasma EUV source based on a gas-puff target for studies of thin silicon membrane and NaCl crystals morphology. Our motivation is to test the recently developed EUV microscopy setup on non-trivial objects. Previously measured spatial resolution of this microscope reaching 50 nm allows for acquisition of images of the membranes and salt crystals with high spatial resolution and field of view approaching $50 \times 50 \mu\text{m}^2$ in a very compact setup. Utilization of the short wavelength EUV radiation allows demonstrating the intrinsic advantage of this radiation for extraction of additional information about the investigated object, which cannot be obtained directly from optical micrographs and SEM images. Moreover, this microscope does not require additional sample modification necessary for SEM microscopy.

2 Experimental setup

The EUV microscope was equipped with an ellipsoidal mirror with Mo/Si coating to focus extreme ultraviolet (EUV) radiation onto an object. A Fresnel zone plate (FZP) objective was used to form a magnified image onto a EUV-sensitive CCD camera in the transmission mode. The use of the gas-puff target eliminates the debris production problem associated with solid targets. Quasi-monochromatic EUV radiation, which is required for the use of Fresnel optics, was produced by spectral selection of a single line emitting at 13.8 nm wavelength from argon plasma. So far, different test objects (samples) were imaged with this setup: Cu mesh with

thickness of $\sim 4 \mu\text{m}$ [4] and carbon foil, 70 nm thick, with holes [5], where the EUV images have been obtained with the half-pitch spatial resolution approaching ~ 50 nm (3.7λ) in a very compact setup. The scheme and experimental arrangement are shown in Fig. 1a) and a photograph of the EUV microscope is shown in Fig. 1b).

The laser plasma EUV source, used in the experiment, has been developed for EUV metrology applications in the frame of the MEDEA+ project [13] and later modified for quasi-monochromatic emission in the 13–14 nm wavelength range, described in detail elsewhere [14]. This source has the advantage over other compact sources that simply by choosing a suitable gaseous target it is possible to change both the peak emission wavelength and the inverse relative bandwidth of the emission from the plasma. Moreover, the gaseous target does not produce any debris associated with solid targets.

Ar plasma was produced by Nd:YAG laser (Eksma) irradiation of a gaseous target with pulse duration of 4 ns, wavelength 1,064 nm, and energy 0.74 J. The plasma radiates in a very broad range of wavelengths, dominantly in the EUV range (5–50 nm wavelength). By using additional spectral filtering, it is possible to shape the spectral emission of the source. The source can operate at up to 10 Hz repetition rate. A pressure of 2×10^{-3} mbar was constantly maintained in the chamber during the source operation.

EUV radiation from the plasma was both focused and spectrally filtered by a Mo/Si multilayer ellipsoidal mirror (condenser) with 80 mm in diameter. The mirror was developed in collaboration with Reflex s.r.o. (mirror substrate) and Fraunhofer Institut für Angewandte Optik und Feinmechanik (coating). The multilayer coating was optimized for 13.5 ± 0.5 nm (FWHM) wavelength range and

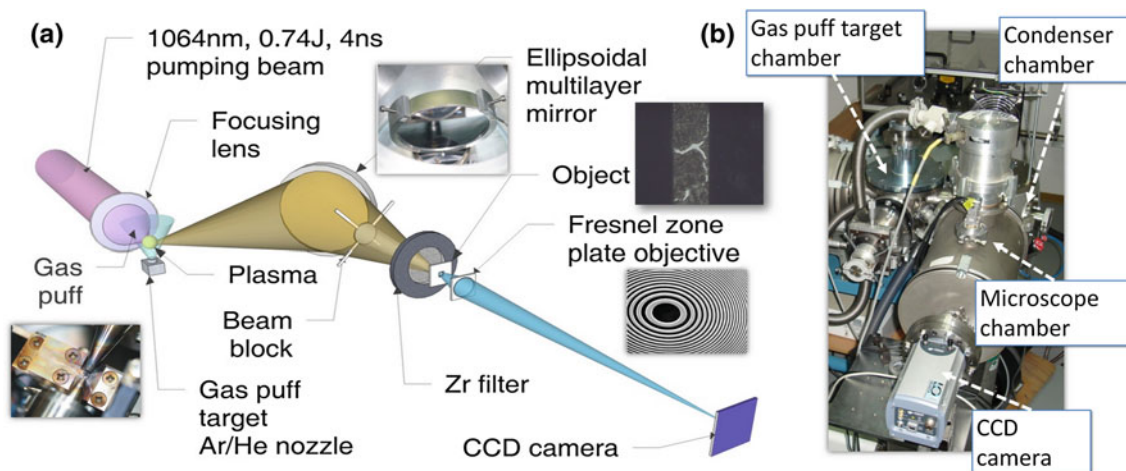


Fig. 1 a Scheme (not to scale) and b photograph of the EUV microscope using a laser-plasma EUV source based on gas-puff target

45 degrees incidence angle. The theoretical reflectivity of the mirror is 37.7 % at 13.5 nm wavelength for an unpolarized light.

The laser plasma source was optimized for efficient generation of EUV radiation from Ar plasma. The in band ($\lambda = 13\text{--}14$ nm) photon flux was $(8.8 \pm 0.5) \times 10^{10}$ photons per pulse in a horizontally elongated spot with a size 1.09×0.39 mm² (FWHM) [14]. That corresponds to the energy of 1.29 $\mu\text{J}/\text{pulse}$.

To eliminate longer wavelengths ($\lambda > 18$ nm), a 100 nm thick, 10 mm diameter, free-standing Zr filter (Lebow) was used. The Zr filter was positioned $\sim 4\text{--}5$ mm upstream the object. A quasi-monochromatic spectrum was obtained from Ar plasma after spectral filtration by the condenser. The resulting spectrum has two main peaks at 13.793 and 13.844 nm wavelength—transitions in Ar^{VIII} [15]. The inverse relative bandwidth (FWHM) of the filtered spectrum is $\lambda/\Delta\lambda = 140$ at $\lambda = 13.84$ nm.

As an object, we used NaCl crystallized on a 15-nm thick non-porous silicon membrane (SPI Supplies) with dimensions 0.07×1.5 mm². The substrate—a silicon wafer 3×3 mm² in size and 100 μm thick—contains two rectangular shape membrane windows. The NaCl crystals were prepared from phosphate buffered saline (PBS) solution (Lonza, Cat.No. BE17-516Q, contents KH₂PO₄ 144 mg/L, NaCl 9000 mg/L, Na₂HPO₄ 795 mg/L). 5 μl of the solution was deposited onto the membrane. The water from the solution was evaporated at the temperature of 21 °C and atmospheric pressure, resulting in re-crystallization of NaCl. During the process of re-crystallization, stress was introduced to the membrane causing random cracks of various sizes to appear in the NaCl crystals and the silicon membrane. Optical images of the object obtained with 40 \times (NA = 0.65) and 100 \times (NA ~ 1) objectives are shown in Fig. 2a and b, respectively.

The object, placed 254 mm from the condenser mirror, is imaged using a FZP objective (Zone Plates Ltd.) onto a EUV sensitive CCD camera iKon-M (Andor) with $1,024 \times 1,024$ pixels and 13×13 μm^2 pixel size. The diameter of the FZP is $D = 200$ μm , number of zones $N_{\text{FZP}} = 1,000$ and an outer zone width $\Delta r = 50$ nm [The ZP was fabricated by Zone Plates Ltd., using electron beam lithography in 220 nm thick PMMA (polymethyl methacrylate) layer spin-coated on top of a 50 nm thick silicon nitride Si₃N₄ membrane]. The FZP was fabricated and optimized for $\lambda = 13.5$ nm. In the case of quasi-monochromatic illumination at $\lambda = 13.84$ nm from Ar plasma, the focal length of the FZP is $f = 722.5$ μm and the numerical aperture NA = 0.138. The depth of focus (DOF), calculated as $\text{DOF} = \pm\lambda/(2\text{NA}^2)$ is equal to ± 363.4 nm. Typically, the magnification is equal to 520 \times (FZP magnification), adjusted by changing the camera-to-FZP distance and refocusing. This results in 25.9×25.9 nm² pixel size and the field of view 26.4×26.4 μm^2 . More information regarding the EUV microscope can be found in [4, 5]. Geometrical numerical apertures of the condenser mirror in the horizontal and vertical directions are equal to $\text{NA}_{\text{CH}} = 0.11$ and $\text{NA}_{\text{CV}} = 0.15$, respectively. They are similar to the numerical aperture of the FZP, $\text{NA}_{\text{FZP}} = 0.138$. Since $\sigma_{\text{H,V}} = \text{NA}_{\text{CH,V}}/\text{NA}_{\text{FZP}}$ are equal to $[\sigma_{\text{H}}, \sigma_{\text{V}}] = [0.8, 1.1]$, the sample is incoherently illuminated [16]. The FZP was mounted on a three axis translation stage driven by vacuum compatible step motor actuators (Standa). A piezoelectric single-axis flexure stage (Thorlabs, model NF15A) with 25 μm travel was used to adjust precisely the object-to-FZP distance at a rate of 3 V/ μm , to locate the image plane with position accuracy better than the DOF. In our case, the theoretical resolution of the piezo-stage was ~ 10 nm \ll DOF. A circular beam block with 12 mm in diameter was placed ~ 15 cm from

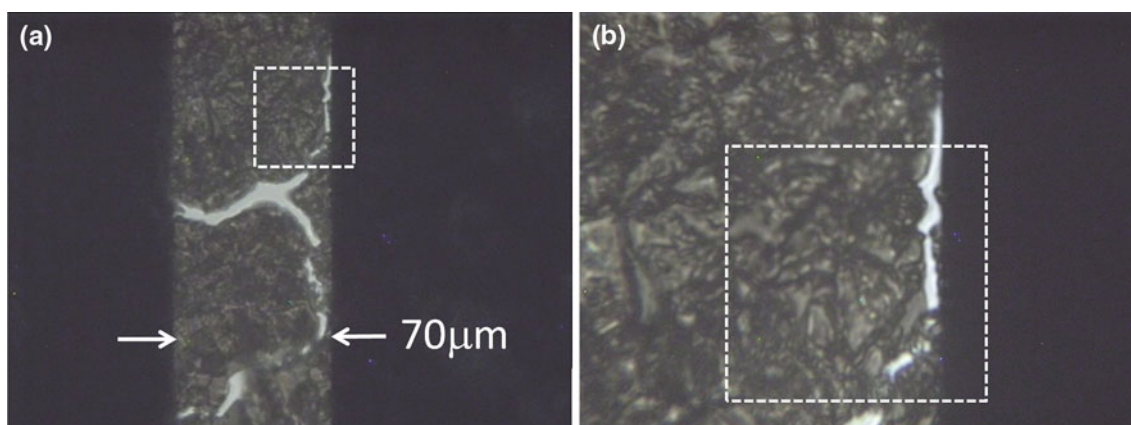


Fig. 2 Optical images of thin Si membrane with NaCl crystals deposited on top with **a** 40 \times (NA = 0.65), **b** 100 \times (NA ~ 1) objectives. Dashed boxes indicate the size of object region imaged with the EUV microscope

the FZP to achieve a conical illumination of the object and avoid stray light through the FZP.

In the case of “binary” transmission, test objects such as Cu mesh, 25–50 EUV pulses at 2 Hz repetition rate were necessary to obtain a single image [5]. The required exposure for imaging of NaCl crystals deposited on the silicon membrane was 200 EUV pulses at 2 Hz. The source can operate at up to 10 Hz repetition rate; however, the pressure buildup in the microscope chamber might cause re-absorption of EUV photons in neutral gas. Therefore, the lower repetition rate was used for image acquisition. The CCD camera was cooled down to $-20\text{ }^{\circ}\text{C}$ to decrease intrinsic noise during the image acquisition.

For the purpose of comparison, the same area of the sample was imaged with a SEM microscope (Tescan VEGA II SBU) and with the EUV microscope described above. SEM image was obtained after deposition of $\sim 10\text{ nm}$ of Au to avoid charging during image acquisition at 30 kV at magnification of $\sim 4,000\times$ (sample to screen magnification).

3 Experimental results

From Fig. 2, it is clear that the cracks in the thin silicon membrane are usually quite large, in the range of one to tens of microns. Crystal film, however, has also a variable transmission to the visible light, but except that, nothing else can be concluded about the object. To obtain more information, the same object was imaged using SEM and EUV microscopes.

The SEM image of the membrane with NaCl crystals on top is shown in Fig. 3a. The same region was also imaged with the EUV microscope. To observe the same area, EUV image was produced by stitching of 16 partially overlapping images in a 4×4 array, which can be seen in Fig. 3b. Each image was obtained by precise adjustment of the object-to-ZP distance, using a previously mentioned piezo actuator, with position accuracy of 300 nm, smaller than the DOF. It was necessary to satisfy this condition, because otherwise the EUV image will be out of focus and will have lower spatial resolution. The area of both SEM and EUV images is approximately $50 \times 50\text{ }\mu\text{m}^2$. The same region is also indicated in Fig. 2 with dashed boxes. The SEM image in Fig. 3a shows NaCl crystals in detail. Their complex structure obscures, however, the information about the membrane itself. In the SEM image, it is possible to see dents, cracks, and pits in the sample, but in some cases, it is not possible to determine how deep they are.

The EUV mosaic shown in Fig. 3b, on the other hand, does not reveal any surface features formed by the thick layer of crystallized salt. The crystals are several microns thick and their transmission at EUV wavelength of 13.8 nm is $\sim 1.5 \times 10^{-7}$ (Assumed NaCl thickness was 1 μm , using CXRO database, http://henke.lbl.gov/optical_constants/filter2.html). However, the EUV image shows regions with thickness smaller than $\sim 100\text{ nm}$ that are represented by the bright regions. These are formed by very deep gaps in the NaCl layer and small cracks and holes in the supporting Si membrane. Intensity of these regions is related to their transmission and, as can be seen in Fig. 3b, some regions have higher transmission than the others. Despite the images are rather noisy, they confirm that EUV microscopy can be

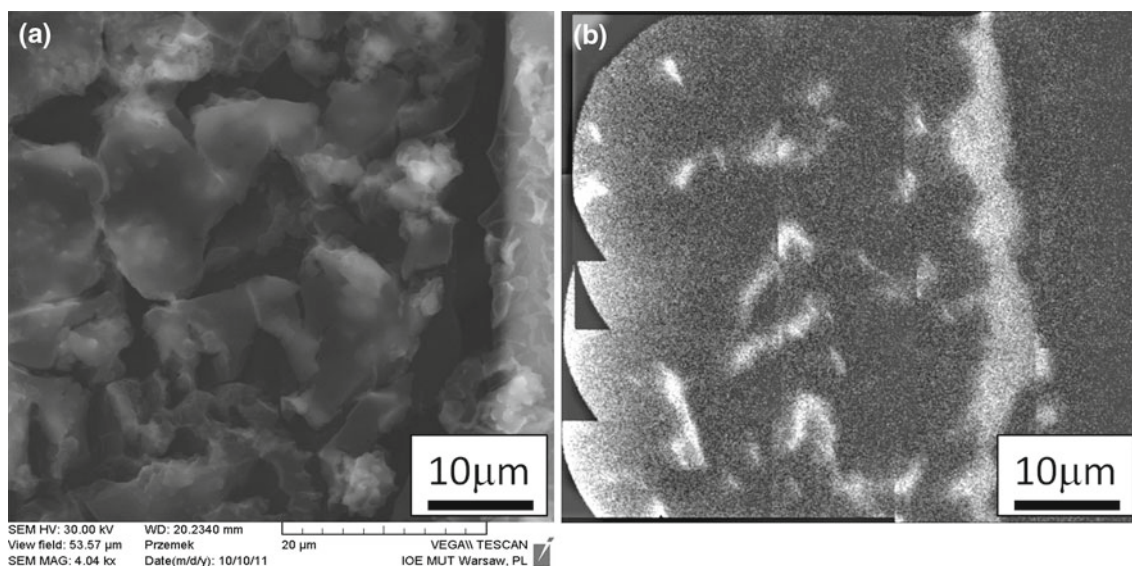


Fig. 3 SEM image of the sample, $\sim 50 \times 50\text{ }\mu\text{m}^2$ with re-crystallized NaCl (a) and corresponding EUV image (b) showing the same region of the sample. EUV image was obtained by stitching and partially overlapping of 4×4 smaller EUV sub-images

used, for example, in thin film studies with several advantages. Figure 3 shows that the EUV radiation used for image acquisition enhances some information about the object which is also present in the SEM image, however, more difficult to extract. The brightest regions indicate cracks in the supporting membrane, as can be observed comparing images of a 2–8 μm wide vertical crack, shown in top-right region of a dashed box in Fig. 2b and on the right in Fig. 3b. Other, less intense features are also visible suggesting lower object transmission and, in turn, higher thickness.

Another interesting fact is that there are some features, which are marked with white arrows that are visible in both SEM and EUV images presented in Fig. 4a, b. However, there are also some cracks in the crystal film, visible in the SEM image, such as one marked with dotted arrow, but not present in the EUV image, as can be seen in Fig. 4c, d. Again, on the left SEM images are shown and on the right are corresponding EUV images of exactly the same regions of the sample. Interestingly, some features, such as the cracks in Fig. 4a and in Fig. 4d, are almost indistinguishable in the SEM images. Corresponding EUV images, on the other hand, show completely different depth of these features. One of them, shown in Fig. 4a, is undoubtedly all the way to the supporting membrane, while another crack in Fig. 4d is only a near-surface feature. Thus, in this case, the EUV radiation enables additional, complementary information about the object to be obtained, which is based on an intrinsic property of EUV light, and that cannot be obtained directly using SEM microscopy or visible light microscopy.

Images obtained with test samples generally exhibit higher signal-to-noise ratio (S/N) than images of non-trivial samples. Moreover, the EUV source photon flux is often insufficient. In addition, the sample, used in this study, although is suitable to show the advantages of using EUV light, however, is difficult to image, because the only signal are the photons passing through small, sometimes around 100-nm wide, cracks in the membrane. These photons produce an actual image on the CCD camera. This is the reason, why the S/N ratio is not high. Despite that, some nanoscopic features can be recognized in the EUV images.

Typical intensity cross-sections throughout some small features in the EUV images are presented in Fig. 5. The cross-section shown in Fig. 5a, obtained without spatial averaging, clearly indicates the signal associated with a feature ~ 260 nm wide. Moreover, as can be seen in Fig. 5b, features with characteristic size as small as 4 pixels can be resolved. For the given magnification and pixel size of 25.9 nm square, the FWHM width of this small feature approaches 100 nm with S/N ratio of 2.2.

The smallest features, of this non-trivial sample, were observed with spatial resolution that was not measured

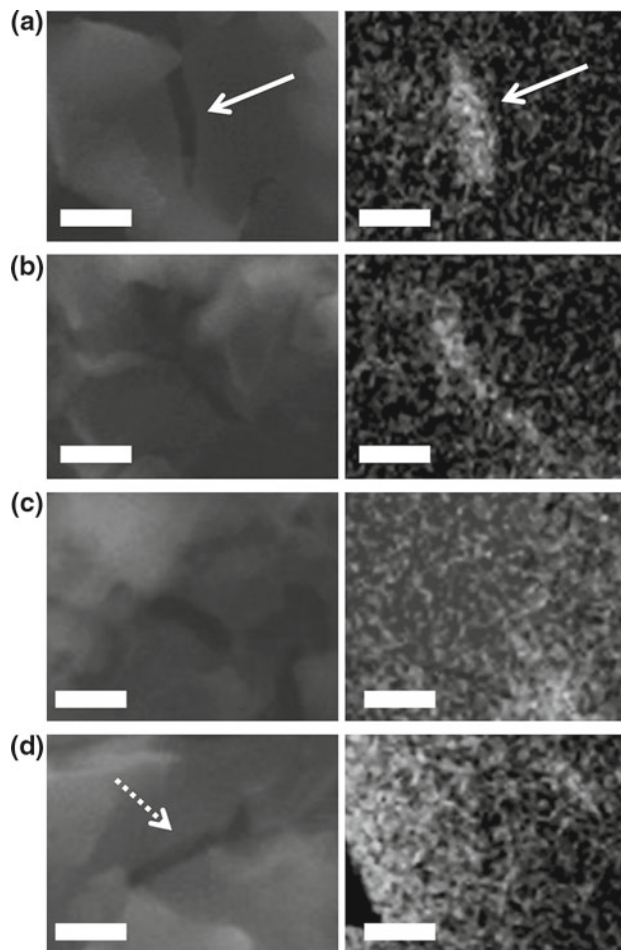


Fig. 4 Comparison between small sections of SEM images (*left column*) and EUV images (*right column*) showing different areas of the sample. **a, b** Some cracks, as small as 100 nm, in the sample are deep all the way to the membrane and can be seen in both SEM and EUV images (marked with *white arrows* and **c, d** some of the features (marked with *dotted arrow*) are visible in the SEM images but are not present in the corresponding EUV image. *Scale bar* is 2 μm

directly using knife-edge test. It is due to the fact, that this sample does not have a proper edge, required by the knife-edge resolution test. However, we can say that the obtained resolution is comparable to the resolution measured with test samples. The half-pitch spatial resolution, reported previously using test samples, was ~ 50 nm, while the smallest visible feature width is approximately twice that value, ~ 100 nm, corresponding to a full pitch spatial resolution, or Rayleigh resolution. The theoretical resolution for the microscope system, taking into account the ZP outerzone width of 50 nm, is limited by the zone plate objective to half-pitch spatial resolution equal to ~ 30 nm, for monochromatic illumination. For actual, quasi-monochromatic illumination EUV microscope half-pitch spatial resolution was previously, assessed with test samples and reported to be ~ 50 nm [5].

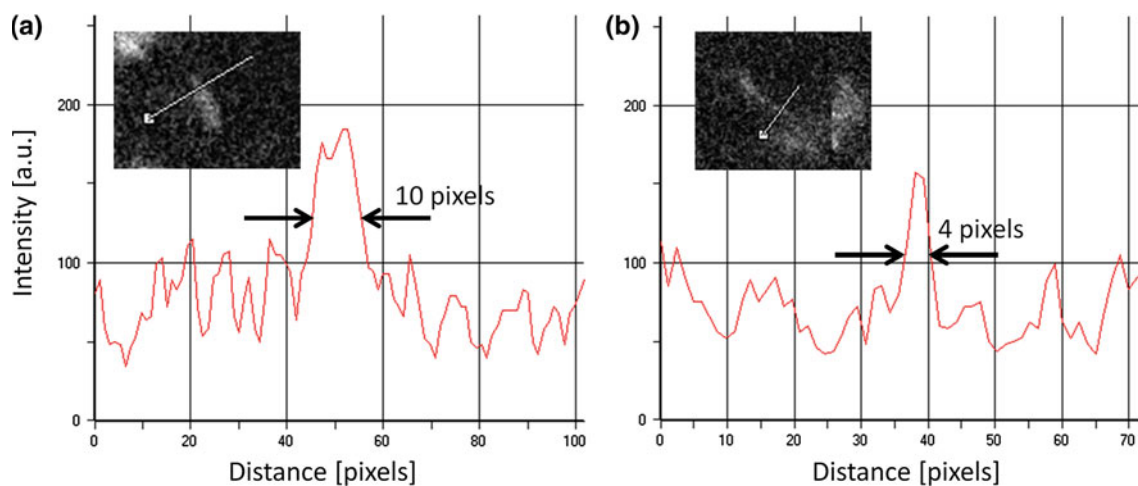


Fig. 5 Intensity profiles of smallest features in the EUV images (a) showing visible features as small as 4 pixel wide (b)

4 Conclusions

This paper demonstrates imaging of nanostructures using a desktop EUV transmission microscope based on laser-produced plasma from a gas-puff target and Fresnel optics. Features with characteristic dimensions as small as 100 nm were resolved.

In addition, we showed that EUV light allows straightforward extraction of meaningful information about sub-100 nm thin films by a direct observation. No specific sample modification is required, such as conductive coating for the SEM. The short attenuation length of EUV photons in almost any material can be utilized to determine the thickness of an object with high sensitivity. Thus, EUV microscopy can be employed in thin layer studies providing information complementary to optical and SEM microscopy.

The work presented in this paper was a part of an effort to develop a novel compact high-resolution imaging system that would find applications in material science, biomedicine, nanotechnology, and other fields. Future improvements of the vacuum pumping system will enable increasing the repetition rate to 10 Hz which will reduce the exposure time by a factor of 5. We are also planning to employ a pumping laser providing pulses with higher energy (10 J in 10 ns) which should increase the EUV source photon flux. Moreover, replacing the FZP objective with a larger one having 250 μm in diameter will allow to collect more photons thus improves the throughput of the imaging system, further decreasing the acquisition time. Our plans also include development of a SXR microscope based on Ar or N_2 gas puff target source [17], capable of imaging in the XUV “water window” spectral region.

Acknowledgments The research was supported by the Foundation for Polish Science under the HOMING 2009 Programme (grant

number HOM2009/14B), partially funded by EU from EUROPEAN REGIONAL DEVELOPMENT FUND project number: WND-POiG.02.01.00-14-095/09, Military University of Technology project number 08-662, the EC’s 7. Framework Program (LASERLAB-EUROPE-grant agreement n° 228334 and COST Action MP0601, also co-funded by Polish Ministry of Science and Education, decision number 816/N-COST/2010/0), European Economic Area (EEA) Grants. Also, the support of GA AV CR KAN300100702 project is gratefully acknowledged.

Open Access This article is distributed under the terms of the Creative Commons Attribution License which permits any use, distribution, and reproduction in any medium, provided the original author(s) and the source are credited.

References

1. D. Attwood, *Soft X-rays and extreme ultraviolet radiation* (Cambridge University, Cambridge, 1999)
2. W. Chao, J. Kim, S. Rekawa, P. Fischer, E.H. Anderson, *Opt. Express* **17**(20), 17699 (2009)
3. G. Vaschenko, C. Brewer, F. Brizuela, Y. Wang, M.A. Larotonda, B.M. Luther, M.C. Marconi, J.J. Rocca, C.S. Menoni, *Opt. Lett.* **31**, 1214–1216 (2006)
4. P.W. Wachulak, A. Bartnik, H. Fiedorowicz, *Optics Lett.* **35**(14), 2337–2339 (2011)
5. P.W. Wachulak, A. Bartnik, H. Fiedorowicz, J. Kostecki, *Opt. Express* **19**(10), 9541–9550 (2011)
6. M. Wieland, C. Spielmann, U. Kleineberg, T. Westerwalbesloh, U. Heinzmann, T. Wilhein, *Ultramicroscopy* **102**, 93 (2005)
7. M. Kishimoto, M. Tanaka, R. Tai, K. Sukegawa, M. Kado, N. Hasegawa, H. Tang, T. Kawachi, P. Lu, K. Nagashima, H. Daido, Y. Kato, K. Nagai, H. Takenaka, *J. Phys. IV* **104**, 141 (2003)
8. I.A. Artiukov, A.V. Vinogradov, V.E. Asadchikov, Y.S. Kasyanov, R.V. Serov, A.I. Fedorenko, V.V. Kondratenko, S.A. Yulin, *Opt. Lett.* **20**, 2451 (1995)
9. F. Brizuela, Y. Wang, C.A. Brewer, F. Pedaci, W. Chao, E.H. Anderson, Y. Liu, K.A. Goldberg, P. Naulleau, P. Wachulak, M.C. Marconi, D.T. Attwood, J.J. Rocca, C.S. Menoni, *Opt. Lett.* **34**(3), 27 (2009)

10. C.A. Brewer, F. Brizuela, P. Wachulak, D.H. Martz, W. Chao, E.H. Anderson, D.T. Attwood, A.V. Vinogradov, I.A. Artyukov, A.G. Ponomareko, V.V. Kondratenko, M.C. Marconi, J.J. Rocca, C.S. Menoni, *Opt. Lett.* **33**(5), 518 (2008)
11. K.W. Kim, Y. Kwon, K.Y. Nam, J.H. Lim, K.G. Kim, K.S. Chon, B.H. Kim, D.E. Kim, J.G. Kim, B.N. Ahn, H.J. Shin, S. Rah, K.H. Kim, J.S. Chae, D.G. Gweon, D.W. Kang, S.H. Kang, J.Y. Min, K.S. Choi, S.E. Yoon, E.A. Kim, Y. Namba, K.H. Yoon, *Phys. Med. Biol.* **51**, N99–N107 (2006)
12. L. Juschkin, R. Freiberger, K. Bergman, *J. Phys. Conf. Ser.* **186**, 012030 (2009)
13. H. Fiedorowicz, A. Bartnik, R. Jarocki, J. Kostecki, J. Krzywinski, J. Mikołajczyk, R. Rakowski, A. Szczurek, M. Szczurek, *J. Alloys Compd.* **401**, 99 (2005)
14. P.W. Wachulak, A. Bartnik, H. Fiedorowicz, T. Feigl, R. Jarocki, J. Kostecki, R. Rakowski, P. Rudawski, M. Sawicka, M. Szczurek, A. Szczurek, Z. Zawadzki, *Appl. Phys. B* **100**(3), 461–469 (2010)
15. R.L. Kelly, *J. Phys. Chem. Ref. Data*, **16**, supplement 1 (1987)
16. J.M. Heck, D.T. Attwood, W. Meyer-Ilse, E.H. Anderson, *J. X-ray Sci Technol* **8**, 95 (1998)
17. P.W. Wachulak, A. Bartnik, H. Fiedorowicz, P. Rudawski, R. Jarocki, J. Kostecki, M. Szczurek, *Nucl. Instrum. Methods Phys. Res. Sect. B* **268**(10), 1692–1700 (2010)